Missing SO_2 Oxidant in the Coastal Atmosphere ? – Observations from High Resolution Measurements of OH and Atmospheric Sulfur Compounds

H. Berresheim, M. Adam, C. Monahan, C. O'Dowd,

School of Physics & Centre for Climate and Air Pollution Studies,

National University of Ireland Galway, Ireland

J.M.C. Plane,

School of Chemistry, University of Leeds, United Kingdom,

B. Bohn, and F. Rohrer*

Institute for Energy and Climate Research (IEK-8), Research Center Jülich, Germany.

Revised version submitted to Atmospheric Chemistry and Physics (ACP)

*corresponding author

Abstract

Diurnal and seasonal variations of gaseous sulfuric acid (H_2SO_4) and methane sulfonic acid (MSA) were measured in N.E. Atlantic air at the Mace Head atmospheric research station during the years 2010 and 2011. The measurements utilized selected ion / chemical ionization mass spectrometry (SI/CIMS) with a detection limit for both compounds of 4.3 x 10^4 cm^{-3} at 5 min signal integration. The H_2SO_4 and MSA gas-phase concentrations were analysed in conjunction with the condensational sink for both compounds derived from 3 nm – 10 μm (aerodynamic diameter) aerosol size distributions. Accommodation coefficients of 1.0 for H_2SO_4 and 0.12 for MSA were assumed leading to estimated atmospheric lifetimes of the order of 7 min and 25 min, respectively. With the SI/CIMS instrument in OH measurement mode alternating between OH signal and background (non-OH) signal evidence was obtained for the presence of one or more unknown oxidants of SO_2 in addition to OH. Depending on the nature of the oxidant(s) their ambient concentration may be enhanced in the CIMS inlet system by additional production. The apparent unknown SO_2 oxidant was additionally confirmed by direct measurements of SO_2 in conjunction with calculated H_2SO_4 concentrations. The calculated concentrations were consistently lower than the measured concentrations by a factor 4.7 ± 2.4 when considering the oxidation of SO_2 by OH as the only source of H_2SO_4. Both the OH and the background signal were also observed to increase significantly during daytime aerosol nucleation events, independent of the ozone photolysis frequency, $J(O^1D)$, and were followed by peaks in both H_2SO_4 and MSA concentrations. This suggests a strong relation between the unknown oxidant(s), OH chemistry, and the atmospheric photolysis and photo-oxidation of biogenic iodine compounds. As to the identity of the oxidant(s), we have been able to exclude ClO, BrO, IO, and OIO as possible

candidates based on *ab initio* calculations. Stabilized Criegee intermediates (sCI) produced from ozonolysis of simple alkenes or via direct photolysis of CH_2I_2 potentially contribute to the oxidation efficiency of the coastal and marine atmosphere. However, analysis of the CIMS background signal in context with recently published kinetic data currently suggests that larger sCI produced from ozonolysis of terpenes play no significant role for SO_2 oxidation in the marine atmosphere. The possibilities of H_2SO_4 formation via SO_3 instead of SO_2 as precursor and/or from SO_2 oxidation by small sCI produced photolytically are both consistent with our observations and need to be further explored.

1. Introduction

It has been well established that homogeneous oxidation of tropospheric gases is generally dominated by reactions with the hydroxyl (OH) radical during daylight hours and - in regions with significant nitrogen oxide, NOx, concentrations - with the nitrate (NO_3) radical in the absence of sunlight [Stone et al., 2012]. Reactions of molecular oxygen, ozone, or peroxy radicals such as HO_2 and RO_2 (R = organic rest molecule) are comparatively slow, with few exceptions, such as NO + HO_2 which recycles OH [e.g., Atkinson et al., 2004]. Heterogeneous oxidation (on the surface of aerosol particles and in cloud and fog droplets) is dominated either by reactions with dissolved ozone, hydrogen peroxide, or molecular oxygen, the latter pathway being catalyzed by transition metal ions [Harris et al., 2013; Berresheim and Jaeschke, 1986]. However, recent studies have revived an interest in the formation and fate of atmospheric Criegee intermediates (radical species produced from reactions of ozone with alkenes [Calvert et al., 2000; Criegee, 1975]) which to this day have eluded

direct measurements in the atmosphere since Cox and Penkett [1971] first suggested their potentially important role. Field and laboratory measurements [Berndt et al., 2014; Stone et al., 2014; Taatjes et al., 2014; Berndt et al., 2012; Mauldin et al., 2012; Welz et al., 2012] as well as theoretical and modelling studies [Sarwar et al., 2014; Boy et al., 2013; Vereecken et al., 2012] now suggest that the reactivity of these types of radicals towards compounds such as SO_2 may have been underestimated by at least two orders of magnitude (see also the recent review by Taatjes et al. [2014]). Therefore, in addition to OH - or possibly even rivalling OH chemistry - Criegee intermediates may, under certain conditions, be significant contributors to atmospheric sulfuric acid formation and the production of hygroscopic sulfate particles which can be activated as cloud condensation nuclei (CCN).

Selected ion – chemical ionization mass spectrometry (SI/CIMS) has been pioneered by Eisele and coworkers [Tanner and Eisele, 1995; Eisele and Tanner, 1993, 1991] for high time resolution measurements of OH, H_2SO_4, MSA(g) (gaseous methane sulfonic acid), and other compounds in the troposphere. A large number of field studies both on the ground as well as airborne have been successfully conducted using this technique and significantly improved our understanding of tropospheric chemistry [e.g., Stone et al., 2012; Huey, 2007; Heard and Pilling, 2003]. In some of these studies it has already been conjectured that SI/CIMS may also provide information about the presence of atmospheric oxidants other than OH by analyzing the background signal recordings obtained in the OH measurement mode. Specifically, the identity of those “background X-oxidant(s)” was speculated to be Criegee intermediates because of their observed reactivity towards SO_2 in the measurement system [e.g., Berresheim et al., 2002].

In the present paper we have analyzed two years of SI/CIMS measurements made at Mace Head, Ireland, for significant occurrences of such background signals indicating the presence of one or more unknown oxidants in coastal air which contribute to H_2SO_4 formation by oxidizing SO_2 (in addition to OH) during day- and nighttime. Furthermore, balance calculations of ambient H_2SO_4 levels using measured SO_2, OH, and aerosol particle concentrations have been compared with measured H_2SO_4 levels. This allowed us to approximate corresponding contributions to ambient H_2SO_4 levels from oxidation of SO_2 by oxidants other than OH and estimate their relative importance with respect to OH reactivity.

2. Experimental

A principle scheme of the Mace Head CIMS instrument and its operation is shown in Figure 1. Similar to previously described systems [Berresheim et al., 2013; 2000; Mauldin et al., 2012; 1998] the aerodynamically shaped main air inlet extrudes retractably through the wall of the building, here towards the open ocean with a marine wind sector of 190°-300°. In the following text, "marine sector" data includes only the subset of data consistent with the marine wind sector, NO levels < 50 pptv, and/or black carbon concentrations < 50 ng m^{-3}. From the main air flow (approximately 2.5 m^3 hr^{-1}) the central region is sampled at 12 slpm through a 1.9 cm diameter sample flow tube. Two pairs of oppositely arranged capillary stainless steel injectors (the front pair sitting upflow, the rear pair downflow at 5.2 cm distance from each other) protrude into the sample flow tube. Depending on the operational mode (OH signal measurement, OH background measurement, or H_2SO_4 and MSA(g)

measurement) selected flows of SO_2, propane (C_3H_8), and N_2 (as make-up gas) are added through the injectors to the sample flow.

For measuring an OH signal isotopically heavy $^{34}SO_2$ (98.8%, Eurisotop, Saint-Aubin, France) is introduced through the front injectors and mixed into the sample air flow resulting in a SO_2 mixing ratio of approximately 8 ppmv. At this setting, the OH lifetime (1/e definition) in the sample flow is 6 ms. The ambient OH concentration introduced into the CIMS system is completely converted to $H_2{}^{34}SO_4$ by its reaction with $^{34}SO_2$ within the available reaction time of $\tau_{reac,OH}$ = 78 ms before reaching the rear injectors. Approximately 1% of the resulting product, $H_2{}^{34}SO_4$, is converted via chemical ionization at atmospheric pressure by NO_3^- reactant ions into $H^{34}SO_4^-$ product ions which are then focussed and guided by electrical potentials (along with remaining NO_3^- ions) through a 80 μm aperture into the vacuum mass spectrometry region. The reactant ions are produced in a sheath flow of purified ambient air with added HNO_3 passing by a radioactive ^{241}Am alpha emitter (activity: 4.1 MBq; Eckert & Ziegler, Berlin, Germany). Detection of the $H^{34}SO_4^-$ signal at m/z 99 following quadrupole mass filtering yields the equivalent concentration of OH in ambient air. Applying the same method of ionization, ambient sulfuric acid, H_2SO_4, and methane sulfonic acid, CH_3SO_3H, in which sulfur occurs as ^{32}S at a fraction of 0.95 [Krouse and Grinenko, 1991] are detected at m/z 97 and m/z 95, respectively. Time resolution for measuring all three masses is typically 30 s. In general, measurement signals are integrated to 5 min with corresponding detection limits of 1.3 x 10^5 cm^{-3} for OH and 4.3 x 10^4 cm^{-3} for both H_2SO_4 and MSA(g), respectively [Berresheim et al., 2013; Mauldin et al., 1998]. Further details including calibration procedures can be found in Berresheim et al. [2000].

126 Propane (99.95%, Air Liquide, UK) is introduced into the sample flow
127 through the rear injectors (establishing a mixing ratio of approximately 430 ppmv in
128 the sample flow) to scavenge any OH which might be recycled from peroxy radicals
129 via reaction with nitric oxide, NO. On average, nighttime OH measurements showed
130 no statistical difference between the background signal and the OH signal suggesting
131 any potential interference by trace contaminants in the propane to be negligible. Due
132 to similar rate constants for SO_2 and propane with respect to their reaction with OH
133 (both ca. 1 x 10^{-12} cm^3 s^{-1} at 298 K; Atkinson et al. [2004]) any (recycled) OH
134 molecules are completely scavenged by propane instead of SO_2 from this point, i.e.,
135 downflow from the rear injectors. Due to the very low NO mixing ratios in marine air
136 at Mace Head [Berresheim et al., 2013] contributions to the measurement signal from
137 the recycling of OH are expected to be negligible.
138
139 The background (BG) signal in the OH measurement mode is evaluated by switching
140 the propane flow from the rear to the front injectors. This prevents formation of
141 $H^{34}SO_4^-$ ions resulting from $^{34}SO_2$ + OH reaction in the system. Theoretically, any
142 background counts observed at m/z 99 under these conditions should only reflect the
143 4.2% fraction of ^{34}S occurring in ambient H_2SO_4. If a significantly higher BG count is
144 observed this might indicate the presence of a compound with stronger electron
145 affinity than HNO_3 ending up as a product ion at m/z 99. However, experiments
146 conducted without $^{34}SO_2$ in the system never showed any evidence for the existence
147 of such a compound. Therefore, observations of significant BG signals (above the
148 ambient 4.2% $H^{34}SO_4^-$ signal) suggested the presence of one or more unknown
149 oxidants converting $^{34}SO_2$ to $H_2{}^{34}SO_4$ in the CIMS system without appreciably
150 reacting with propane. Indeed this interpretation was corroborated by stopping the

151 SO_2 injection to the sample flow and observing a corresponding reduction in the m/z
152 99 BG signal. Furthermore, with SO_2 in the system, the propane flow through the
153 front injector was successively increased from zero to the operational setting for
154 measuring the BG signal. Before reaching this setting the signal was found to tail off
155 to a background level corresponding to the complete removal of OH. Increasing the
156 propane flow did not further alter the BG signal.
157
158 The total reaction time $\tau_{reac,X}$ available to this unknown oxidant "X" to react with SO_2
159 in the system forming H_2SO_4 is the time starting when a unit volume of the sample
160 flow passes the position of the first injector pairs until it reaches the end of the
161 atmospheric pressure ionization region, i.e., the 80 μm aperture (see Figure 1). That
162 time in our system corresponds to 0.45 s, or approximately half a second, which is
163 about six times longer than $\tau_{reac,OH}$. Therefore, the relative importance of X in
164 comparison to the atmospheric oxidation efficiency of OH may have to be
165 downscaled dependent on the properties of X and its potential formation and/or
166 regeneration during the reaction time. This will be examined in detail in the following
167 section.
168
169 Photolysis frequencies of ozone, $J(O^1D)$, and of nitrogen dioxide, $J(NO_2)$, were
170 measured since September 2010 on top of a 10 m tower next to the laboratory
171 building. Both were exchanged with recalibrated systems on a semiannual basis.
172 Details of the measurement principles and performance of the radiometers have been
173 given by Bohn et al. [2008]. SO_2 was measured in May-August 2011 with a Thermo
174 Systems 43i instrument using a heated sample inlet teflon tubing (40 ºC) to avoid SO_2
175 losses due to water condensate. Based on a cycle of 30 min signal and 30 min zero

176 measurements (with an added active charcoal filter) we calculated a 2σ detection limit
177 of 25 pptv for one hour time integration.
178
179 **3. Results and Discussion**
180
181 **3.1. Seasonal cycles and atmospheric lifetimes of H_2SO_4 and MSA(g)**
182
183 Figure 2 shows the mean seasonal cycle of the daily maximum H_2SO_4 concentration
184 in the marine sector at Mace Head which typically occurred between 1000-1400 UTC
185 local time, depending on cloud cover. In general, H_2SO_4 showed a clear diel variation
186 closely correlated with the OH concentration (Fig. 3, top). The reason for this
187 correlation was the relatively homogeneous mixing ratio of the major precursor, SO_2,
188 in the marine atmosphere, as shown for a three months period in Figure 4 (top), and
189 the relatively short lifetime of H_2SO_4 caused by uptake onto aerosol surfaces. This so
190 called condensational sink (CS) showed also low variability on most days (Fig. 4,
191 bottom). The mean SO_2 mixing ratio in the open ocean sector was 160 (± 50) pptv
192 during these summer months. The average atmospheric lifetime of H_2SO_4 with respect
193 to CS was estimated from scanning mobility particle sizer (SMPS) and aerodynamic
194 particle sizer (APS) measurements using the approach of Fuchs and Sutugin [1971]
195 and Pandis and Seinfeld [1998] to be on the order of 7 minutes assuming an
196 accommodation coefficient of 1.0 [Kolb et al., 2010; Hanson, 2005; Boy et al., 2005],
197 a diffusion coefficient for $H_2SO_4(2\ H_2O)$ of 0.075 atm cm^2 s^{-1} at 75-85% relative
198 humidity [Hanson, 2005], a mean free path of 105 nm for $H_2SO_4(2\ H_2O)$
199 (corresponding to the Fuchs and Sutugin parameterization), and a hygroscopic growth
200 factor of 1.7 (max. 2.0; 90% RH vs. ≤40% RH) [Bialek et al., 2012]. The variability

of CS shown in Figure 4 was mainly driven by particle counts, not relative humidity which mostly ranged between 75-85%. Overall, we estimate that CS values can be uncertain by at least a factor of two, mainly due to the uncertainties in the count rates of the SMPS and APS instruments and of the hygroscopic growth factor.

For Mace Head we assume that except perhaps in winter the predominant source for H_2SO_4 in the marine atmosphere is ultimately biogenic [Lin et al., 2012; Seguin et al., 2010], i.e., the emission and oxidation of dimethyl sulfide (DMS) by OH which yields – via further oxidation of intermediate compounds – the gaseous end products H_2SO_4, dimethyl sulfone ($CH_3SO_2CH_3$, $DMSO_2$), and methane sulfonic acid (CH_3SO_3H, MSA) [Berresheim et al., 1995; 1993a]. As described in the previous section, the two acid compounds are detectable by SI/CIMS using the same instrumental setting as for the OH measurement. Corresponding seasonal cycles of aerosol MSA and non-sea salt sulfate, nss-SO_4, have been measured at Mace Head using high-resolution time-of-flight aerosol mass spectrometry (HR-TOF-MS). Both aerosol compounds as well as their concentration ratio show a clear seasonal maximum in summer [Ovadnevaite et al., 2014].

The mean seasonal cycle of peak MSA(g) mixing ratios recorded during the same daily time slot as for H_2SO_4 and summarized as monthly means is also shown in Figure 2. Similar to H_2SO_4 and the aerosol sulfur compounds, the highest gas phase MSA(g) levels in the marine atmosphere were observed during the summer months which corroborates the biogenic origin of H_2SO_4 measured in this sector. Adopting a sticking coefficient of 0.12 for the aerosol scavenging of MSA(g) [De Bruyn et al., 1994] we obtained an average atmospheric lifetime of approximately half hour (25

226 min) for this compound. As for H_2SO_4 this is somewhat shorter than previously
227 estimated from measurements off the north-western coast of the United States
228 [Berresheim et al., 1993b], however, still within the same order of magnitude.
229 Ammann et al. [2013] have questioned the earlier results obtained by De Bruyn et al.
230 [1994] and Schweitzer et al. [1998] for the MSA(g) accommodation coefficient and
231 suggested preferring a value close to one as reported in the most recent study by
232 Hanson [2005]. However, in our view, adopting a unity value would be in
233 contradiction to common observations of a relatively slower decline of atmospheric
234 MSA(g) levels in comparison to H_2SO_4 in late afternoon and evening hours which has
235 been well documented in previous field studies [e.g., Eisele and Tanner, 1993] and in
236 our present study. Furthermore, as shown already in a previous campaign at Mace
237 Head [Berresheim et al., 2002], ambient MSA(g) levels typically increased with
238 decreasing relative humidity, including at nighttime. Both observations support that
239 the vapor pressure of MSA(g) is significantly higher compared to H_2SO_4 [e.g.,
240 Kreidenweis and Seinfeld, 1988].
241
242 **3.2. H_2SO_4 mass balance and missing SO_2 oxidant in the marine atmosphere**
243
244 From 2 May to 12 August, 2011, an intensive campaign was conducted at Mace Head
245 including measurements of SO_2. The results allowed the calculation of H_2SO_4
246 concentrations based on its production by SO_2 oxidation by OH and removal due to
247 condensation on existing aerosol surface (CS, condensational sink rate) assuming
248 steady state:
249

250 $$[H_2SO_4]_{calc} = \frac{k_{OH}[SO_2][OH]}{CS} \quad (1)$$

Comparison with measured H_2SO_4 concentrations showed a significant underestimation using eq. (1), bearing in mind the uncertainty in CS can be a factor of two. For all measurement days of the campaign, the mean ratio, i.e., $[H_2SO_4]_{meas}/[H_2SO_4]_{calc}$, was 4.7 (±2.4) during the midday periods of 1000-1400 UTC. This is considerably higher than the mean of 2.4 reported by Mauldin et al. [2012] for a boreal forest site in Finland. An extreme example from 18 June, 2011, is shown in Figure 5a. On average, the measured H_2SO_4 concentrations on this day were a factor of 7 higher than the values calculated by eq. (1) and the background signal shows a strong diel cycle in phase with that of OH. Four-day NOAA HYSPLIT air mass back-trajectories (http://ready.arl.noaa.gov/HYSPLIT.php) in conjunction with MODIS satellite imagery (http://neo.sci.gsfc.nasa.gov) of chlorophyll pigments in surface seawater pointed towards high biogenic sulfur (DMS) contributions to the advected air derived from phytoplankton blooms between Greenland and Iceland. On the other hand, no significant changes were observed in ambient SO_2 levels on the same day. Even higher H_2SO_4 and also MSA(g) concentrations (both in the mid-10^7 cm^{-3} range) were measured on 11 June, 2011, with similar air mass trajectories and SO_2 levels as on 18 June, resulting in a measured/calculated H_2SO_4 ratio of 9. A notable difference between both days was the occurrence of low tide at noon on 18 June whereas high tide prevailed at noon on 11 June, respectively.

A contrasting example is shown in Figure 5b for 10 May, 2011, with a ratio of only 1.8 which in view of the overall uncertainties discussed earlier suggests a nearly closed H_2SO_4 balance based on the SO_2 +OH pathway alone. Weather conditions on that day were strongly anticyclonic with no indication of major contributions from

276 biologically active open ocean regions and with overall low solar insolation, i.e., lack
277 of significant photochemistry. The OH background signal did not significantly vary
278 during the day in contrast to the OH concentration itself which despite low insolation
279 still showed a pronounced diel cycle. However, as shown in Figure 6 (e.g., red line),
280 on the vast majority of marine sector days during the 2010 and 2011 measurement
281 periods both the background signal and the OH signal varied in tune with each other
282 which strongly suggests a photolytic source for the unknown compound(s) producing
283 the BG signal. Clearly a major source of H_2SO_4 in addition to OH oxidation of SO_2
284 was missing in the balance calculation based on eq. (1).
285
286 A similar discrepancy between measured and calculated H_2SO_4 values in the coastal
287 atmosphere of Mace Head was reported previously by Berresheim et al. [2002]. They
288 speculated that the missing source might be DMS oxidation with partial production of
289 SO_3 instead of SO_2 as intermediate, which then readily forms H_2SO_4 with water
290 vapour [Lin and Chameides, 1993]. This possibility would also agree with kinetic
291 pathways hypothesized for the DMS + OH oxidation in which CH_3SO_2 and CH_3SO_3
292 are formed as intermediates, both of which decompose thermally to SO_2 and SO_3,
293 respectively [Berresheim et al., 1995]. Studies at an Antarctic coastal location with
294 strong marine DMS emissions [Jefferson et al., 1998; Davis et al., 1998] reported
295 similar inconsistencies between measured H_2SO_4 levels and SO_2 mixing ratios
296 required to close the mass balance based on SO_2 + OH as the only source, even when
297 assuming a very low H_2SO_4 accommodation coefficient of 0.5. Our results shown in
298 Figures 5a and 5b may be consistent with a significant contribution by marine
299 biogenic DMS emissions to H_2SO_4 levels at Mace Head via intermediate production
300 of a precursor other than SO_2. And this influence may even supersede potential

301 regional contributions from emissions which are dependent on tidal cycles as
302 discussed earlier for the cases of 11 and 18 June, 2011. However, current uncertainties
303 in our knowledge of DMS oxidation chemistry prevent a straightforward explanation
304 for the frequently observed diel cycling of the OH background signal.
305
306 Alternatively, biogenic emissions of, e.g., organic halogens from the regional coastal
307 environment during low tide may produce highly reactive atmospheric compounds
308 contributing to these BG signal variations. Recently, it has been suggested that
309 oxidant(s) in addition to OH might play a significant role in atmospheric H_2SO_4
310 formation, e.g., stabilized Criegee intermediates (sCI) which have been re-evaluated
311 with respect to their potential oxidation of atmospheric SO_2 by Liu et al. [2014], Stone
312 et al. [2014], Welz et al. [2012] and Mauldin et al. [2012]. In the following two
313 sections we investigate the potential importance of SO_2 reactions with some halogen
314 and sCI radicals as sources of H_2SO_4 in addition to the DMS→SO_3 and SO_2 +OH
315 pathways in marine air at Mace Head. The nitrate radical, NO_3, is not expected to be
316 of any importance for nighttime SO_2 oxidation at Mace Head, at least not in air from
317 the marine sector [Berresheim et al., 2013].
318
319 **3.3. Electronic structure calculations on halogen oxide reactions with SO_2**
320
321 Other candidates besides OH acting as SO_2 oxidants might be halogen oxide radicals,
322 however, to our knowledge respective rate constants are available in the literature
323 only for the reactions of IO and ClO with SO_2 [Larin et al., 2000]; DeMore et al.,
324 1997], which are three and six orders of magnitude smaller compared to k_{SO2+OH},
325 respectively. We have made *ab initio* transition state energy calculations for the

reactions of SO_2 with ClO, BrO, IO, and OIO using quantum theory. The hybrid density functional / Hartree-Fock B3LYP method was employed from within the Gaussian 09 suite of programs [Frisch et al., 2009], combined with an appropriate basis set for I [Glukhovtsev *et al*., 1995] and the standard 6-311+g(2d,p) triple zeta basis sets for Br, Cl, O and S. The geometries, rotational constants, vibrational frequencies and relative energies of the transition states are listed in Table 1. Following geometry optimizations of the transition states for the reactions of ClO, BrO, IO and OIO with SO_2, and the determination of their corresponding vibrational frequencies and (harmonic) zero-point energies, energies relative to the reactants were obtained. In the case of BrO and ClO + SO_2, more accurate transition state energies were computed at the CBS-QB3 level [Montgomery et al., 2000]. At this level of theory, the expected uncertainty in the calculated transition state energies should be better than 0.07 eV [Foresman and Frisch, 1996]. Spin-orbit effects were ignored since these are present both in the reactant halogen oxide and the transition state. Figure 7 illustrates the transition state geometries for ClO, BrO, IO and OIO + SO_2.

Transition state theory (TST) calculations were then carried out using the calculated molecular parameters in Table 1. Although the reaction between IO and SO_2 has a small barrier (7.3 kJ mol^{-1}), the reaction has quite a tight transition state and the TST calculation yields $k(200 - 400\ K) = 4.3 \times 10^{-14} \exp(-1150/T)$ $cm^3\ s^{-1}$. The resulting value of $k(343\ K) = 1.6 \times 10^{-15}$ $cm^3\ s^{-1}$ is consistent with an experimental upper limit of 6×10^{-15} $cm^3\ s^{-1}$ determined at that temperature by Larin et al. [1998]. At a marine boundary layer temperature of 293 K, the rate coefficient is only 8.5×10^{-16} $cm^3\ s^{-1}$. This reaction would have to compete with OH + SO_2, which has a rate coefficient of $k = 9 \times 10^{-13}$ $cm^3\ s^{-1}$. Although [IO] can be around 30 times larger than [OH] at midday

351 at Mace Head, the ratio of rate constants is 1/1050, so the OH reaction is about 35
352 times faster.
353 During nighttime at Mace Head, OIO builds up to a mixing ratio of a few parts per
354 trillion [Saiz-Lopez and Plane, 2004]. However, the very large barrier for the OIO +
355 SO_2 reaction (50.1 kJ mol^{-1}) means that this reaction is negligibly slow: k(200-400 K)
356 = 6.4×10^{-13} exp(-6400/T) cm^3 s^{-1}, and k(293 K) = 2.2×10^{-22} cm^3 s^{-1}.
357
358 BrO has been observed at a mixing ratio of several parts per trillion during the day at
359 Mace Head [Saiz-Lopez et al., 2004]. However, the reaction BrO + SO_2 also has a
360 significant barrier (20.4 kJ mol^{-1}), and so the reaction is much too slow in the MBL:
361 k(200-400 K) = 5.8×10^{-14} exp(-2700/T) cm^3 s^{-1}, and k(293 K) = 5.6×10^{-18} cm^3 s^{-1}.
362 Finally, the TST calculation for ClO + SO_2, which also has a significant barrier (24.1
363 kJ mol^{-1}), yields k = 5.2×10^{-14} exp(-3100/T) cm^3 s^{-1}. The theoretical rate coefficient
364 at 298 K is therefore 1.5×10^{-18} cm^3 s^{-1}, which is in accord with an experimental
365 upper limit of 4×10^{-18} cm^3 s^{-1} at this temperature [DeMore et al., 1997]. In summary
366 we conclude that none of the halogen oxides considered here exhibit sufficient
367 turnover rates with SO_2 in ambient air to account for the missing H_2SO_4 source .
368
369

370

371 **3.4. Could X be a Criegee radical produced from ozonolysis?**

372

373 Previous measurements at Mace Head have shown clear diurnal cycles of light
374 alkenes (including isoprene) with a strong dependence on solar flux [Broadgate et al.,
375 2004; Lewis et al., 1999]. Assuming that "X" is indeed a Criegee intermediate
376 produced from ozonolysis of alkenes and reacting with SO_2 both in the atmosphere
377 and in the CIMS inlet system to produce additional H_2SO_4, we can estimate its
378 relative contribution compared to the SO_2 +OH reaction as follows.

379

380 As already pointed out in the Experimental section we have to account for additional
381 formation of $[sCI]_{cims}$ from alkene + O_3 reactions over the total available residence
382 time of 0.45 s in the atmospheric pressure reaction and ionization region of the CIMS
383 instrument (see Fig. 1). By continuous reaction with SO_2 and ionization of the
384 resulting $H_2{}^{34}SO_4$ molecules over the corresponding distance (32 cm) this leads to an
385 accumulation of the $H^{34}SO_4^-$ background signal at m/z 99 assuming the sCI+SO_2
386 oxidation to be instantaneous at the high SO_2 concentration in the CIMS reactor tube.
387 The enhancement factor EF relative to the ambient air sCI concentration, $[sCI]_{amb}$, is

388 $$EF_{H_2{}^{34}SO_4} = \frac{[sCI]_{amb} + \int_0^{t_{res}} Prod(sCI) \cdot dt}{[sCI]_{amb}} = 1 + \frac{t_{res}}{\tau_{sCI,amb}} \quad (2)$$

389 This result is the consequence of the fact that both types of sCI, namely sCI produced
390 in ambient conditions ($sCI_{amb} = Prod(sCI) \cdot \tau_{sCI,amb}$) and sCI produced inside the CIMS
391 inlet are immediately converted to $H_2{}^{34}SO_4$ by added $^{34}SO_2$ in the CIMS inlet system.
392 Assuming a lifetime with respect to unimolecular decomposition of 0.2 s for sCI

393 compounds resulting from ozonolysis of the monoterpenes α-pinene and limonene
394 [Mauldin et al., supplement, 2012] and the dominant ambient reaction of sCI with
395 water ($k_{H2O+sCI}$ = 1.4 x 10^{-17} cm^3 s^{-1} (MCM 3.2 http://mcm.leeds.ac.uk/MCM/;
396 Saunders et al. [2003]; Jenkin et al. [2003]), [H_2O] = 3.1 x 10^{17} cm^{-3} representing
397 Mace Head conditions of T = 14 °C, 75% relative humidity) the ambient lifetime of
398 such stabilized Criegee intermediates is estimated to be 0.1 s. As already mentioned,
399 approximately 1% of the H_2SO_4 is ionized in the CIMS ionization region. Therefore,
400 the production of sCI in this region indeed yields H_2SO_4 via reaction with SO_2, of
401 which, however, only 0.5% is ionized, on average, as this process acts linearly.
402 Consequently, we have to modify eq. (2) to take into account the reduced ionization
403 probability for H_2SO_4 produced in the ionization region:
404
405 $$EF_{H^{34}SO_4^-} = 1 + \frac{t_{reac}}{\tau_{sCI,amb}} + 0.5 \cdot \frac{t_{ion}}{\tau_{sCI,amb}} \quad (3)$$

406 with t_{res} = 450 ms, t_{reac} = 115 ms, t_{ion} = 335 ms, $\tau^{-1}_{sCI,amb}$ = 1/0.2 s + 4.3 s^{-1} = 9.3 s^{-1}.
407 This formalism is identical to that derived for a similar instrument by Berndt et al.
408 [2012] (chemical ionization time-of-flight mass spectrometer with atmospheric
409 pressure inlet; CI-APi-TOF-MS). Thus, from eq. (3) it follows that $^{34}SO_2$ oxidation by
410 sCI contributes a background signal which represents an enhancement of the ambient
411 sCI concentration by a factor EF = 3.6. Therefore, if X is indeed a sCI compound (of
412 the kind considered here), the measurement signal resulting from sCI would have to
413 be weighted by 1:3.6 with respect to the OH signal to obtain the corresponding
414 ambient air [sCI] concentration. To compare both compounds with respect to their
415 oxidation efficiency towards SO_2, the corresponding rate constants must be factored
416 in as well, i.e., $k_{sCI+SO2}$ / k_{OH+SO2} = 6 x 10^{-13} cm^3 s^{-1}/ 9 x 10^{-13} cm^3 s^{-1} = 0.67, with

417 k_{OH+SO2} (298 K) = 9 x 10^{-13} cm^3 s^{-1} taken from Atkinson et al. [2004] and $k_{sCI+SO2}$
418 adopted for the (monoterpene + SO_2) reaction as reported by Mauldin et al. [2012].
419 This means that the oxidation efficiency of those sCI compounds would be only on
420 the order of 1:5.4, i.e., 20% compared to that of OH with respect to SO_2 oxidation,
421 assuming that the CIMS background signal is equal to the OH signal as observed on
422 average in the ambient air measurements at Mace Head (see Fig. 6).
423
424 These calculations depend strongly on the kinetic parameters for the corresponding
425 sCI reactions. In this work we have adopted rate constants published by Mauldin et al.
426 [2012] and Berndt et al. [2012] for stabilized Criegee intermediates produced from
427 ozonolysis of monoterpenes. However, other studies of smaller Criegee intermediates
428 with low internal energies (CH_2OO by Stone et al. [2014] and Welz et al. [2012];
429 CH_3CHOO by Taatjes et al. [2013]) suggest much faster reactions of these CI species
430 with both SO_2 and H_2O, respectively. For a sensitivity test we take the parameters
431 from Taatjes el al. [2013], ($k(CI+SO_2)$ = 6.7x10^{-11} and 2.4x10^{-11} cm^3 s^{-1}, $k(CI+H_2O)$ =
432 1x10^{-14} and an upper limit of 4x10^{-15} cm^3 s^{-1} for the *anti* and *syn* conformers of
433 CH_3CHOO, respectively) and neglect the fact, that for the conditions in the CIMS
434 inlet only 80% of these CI would react with the added $^{34}SO_2$. We also neglect their
435 unimolecular decomposition whose rate constant is given as an upper limit of 250 s^{-1}
436 by Taatjes et al. [2013], since this process would make only a small contribution to
437 our estimates. We find that the oxidation efficiency of such CIs – if formed via
438 ozonolysis - compared to OH would be approximately 1:11.8 for *anti* and 1:13.2 for
439 *syn* conformers of CH_3CHOO in contrast to our earlier estimate of 1:5.4, again based
440 on the condition of equal CIMS background and OH signal counts. The relatively
441 small difference between these estimates is a consequence of the fact that both

442 reaction parameters (for CI+SO_2 and CI+H_2O) are faster in this second estimate. The
443 effect of a faster reaction of CI with SO_2 is almost exactly cancelled out by the faster
444 reactions with H_2O. A similar estimate for CH2OO was not done since their time
445 scale for unimolecular decomposition is not known to us.
446
447 For these reasons, if the oxidant(s) X would be such types of stabilized Criegee
448 intermediates, the combined oxidation efficiency of both compounds is estimated to
449 account for a factor of approximately 1.2, increasing the calculated H_2SO_4
450 concentration based on the SO_2 + OH source alone by only 10-20%. This is still a
451 major shortfall with respect to the average factor of 4.7 required to match the
452 observed ambient air H_2SO_4 concentration. Assuming a (rather unlikely) H_2SO_4
453 accommodation coefficient as low as 0.5 would reduce this discrepancy by only 30%.
454 As discussed earlier, we assume that much of the uncertainty remains with the
455 calculation of the condensational sink. However, as yet unknown interferences in the
456 CIMS background signal measurements cannot be entirely ruled out. It appears
457 particularly puzzling that the BG signal frequently tracks the OH signal suggesting
458 that X has similar sources and sinks as OH (Fig. 6). Good candidates for the origin of
459 the CIMS background signal are stabilized Criegee intermediates or iodine oxide (see
460 discussion below). The consequence for the ambient H_2SO_4 budget is more complex.
461 Either different Criegee intermediates than those studied so far or an entirely different
462 kind of oxidant for SO_2 or a production process converting a sulfur compound other
463 than SO_2 might be still missing in our present account of the H_2SO_4 concentration in
464 the coastal marine atmosphere.
465

Recently, Taatjes et al. [2014] and Stone et al. [2013] suggested that CH_2OO might be an important intermediate in marine air resulting from both ozonolysis of alkenes and photolysis of CH_2I_2. Studies by Liu et al. [2014], Stone et al. [2014] and Welz et al. [2012] point towards a significant role of this Criegee intermediate for atmospheric SO_2 oxidation. Figures 8a and 8b show examples for several observations we made in relation to coastal aerosol nucleation events during which OH and also both H_2SO_4 and MSA(g) concentrations increased significantly in conjunction with a major increase in the background signal counts for the X-oxidant(s). On 13 May, 2011 (Fig. 8a) the first low tide was centered at about 0700 UTC. Note that no detectable aerosol nucleation (> 3 nm diameter) occurred at this time as insolation was still low, however, some spikes in both OH concentration and the BG signal were already visible. However, a significant nucleation event occurred during the second low tide between 1800 and 2100 UTC with somewhat enhanced H_2SO_4 and MSA(g) concentrations. Both the OH concentration and the BG signal again increased as well. On the next day, 14 May, 2011 (Fig. 8b) these effects are even more pronounced with the tide shifted by about +45 min and two major nucleation events clearly detectable. The peak of the morning event at about 0800 UTC coincided with a major production of both OH and the X-compound (BG signal). Conversely to the preceding day, the evening event showed relatively minor OH and X production due to the tidal shift.

A recent successful H_2SO_4 intercomparison experiment at Mace Head (M. Sipilä and S. Richters, *pers. commun.*, 2013) between the CIMS instrument and a CI-APi-TOF-MS instrument has confirmed that the CIMS indeed measures only the concentration of gaseous "free" (monomeric) H_2SO_4 during nucleation events. With the rapid transition from monomers to multimer clusters in which H_2SO_4 becomes tied up

491 (confined) and not broken down anymore to the HSO_4^- core ions in the CIMS
492 collision dissociation chamber (Fig. 1) a net decrease in ambient H_2SO_4
493 concentrations may therefore be expected. However, as shown in the nucleation
494 events in Figures 8a and 8b, (monomer) H_2SO_4 levels even increased after a certain
495 lag time following the onset of the event. We interpret our observations as strong
496 formation of X-oxidant(s) (e.g., CH_2OO from photolysis of CH_2I_2; Welz et al. [2012])
497 and OH (perhaps via thermal decomposition of sCI; Berndt et al. [2012], Kroll et al.
498 [2001]) followed by rapid oxidation of DMS and SO_2 to form the products H_2SO_4 and
499 MSA(g). Such coastal nucleation events have previously been shown to be induced by
500 photolysis and photo-oxidation of marine iodine compounds emitted mainly from
501 exposed seaweed during low tide [O'Dowd et al., 2002]. Considering again the
502 IO+SO_2 reaction and adopting a rate constant of $k(IO+SO_2) = 8.5 \times 10^{-16}$ cm^3 s^{-1}
503 (section 3.3), we calculate that approximately 8% of atmospheric IO is converting
504 $^{34}SO_2$ to $H_2{}^{34}SO_4$ in the CIMS inlet system, based on a $^{34}SO_2$ mixing ratio of 8 ppmv
505 and a total IO residence time of 0.45 s. Also, it is assumed that IO does not react with
506 propane. Based on eq. (3) the corresponding yield for $H^{34}SO_4^-$ would be reduced from
507 8% to 5%. With this estimate an upper limit for the atmospheric IO mixing ratio can
508 be derived from the corresponding CIMS background signal. We estimate ambient IO
509 levels to be, on average, less than 1.3 pptv at noon time (Fig. 6) and less than 5 pptv at
510 the maximum of the nucleation event shown in Figures 8a and 8b. This is consistent
511 with previous measurements of IO at Mace Head which showed maximum levels up
512 to 5 pptv [Saiz-Lopez et al., 2006; Alicke et al., 1999]. Future studies are required to
513 systematically characterize remaining uncertainties in the CIMS and CS
514 measurements and to verify a possible link between the unknown oxidant(s) and the
515 iodine cycle in the marine atmosphere.

516

517

4. Conclusions

We observed a persistent but relatively low H_2SO_4 background concentration at nighttime (on the order of a few 10^5 cm^{-3}). Also, on some occasions short spikes were observed at nighttime in the background signal during low tide which might suggest short-term emissions of reactive hydrocarbons capable of forming sCI compounds and OH in reactions with ozone. We assume that such processes also happen during daytime but are superimposed by the formation of another major oxidant which shows a similar diurnal pattern like OH. Whether this oxidant might be a Criegee radical with its production mainly determined by strong light-induced emissions of marine hydrocarbon species and/or atmospheric photolysis of iodine species remains an open question. However, we consider it unlikely that α-pinene or limonene are present at significant levels in the marine atmosphere. In forest environments these compounds are also emitted at nighttime resulting in a quite different diurnal cycle of the OH background signal [Mauldin et al., 2012] than we have observed in the coastal atmosphere. For this reason and also based on the currently available kinetic data for the SO_2 oxidation by sCI compounds resulting from these monoterpenes we conclude that at least those specific sCI radicals are unimportant in comparison with the SO_2+OH oxidation in the marine atmosphere. In the present work we have shown that the OH background signal measured with the CIMS instrument provides evidence for the presence of one or more unknown oxidants for atmospheric SO_2 in addition to OH. However, as this oxidant X does not significantly react with propane in the CIMS system, the corresponding X-signal must be corrected to account for additional production inside the CIMS inlet system before evaluating its oxidation efficiency towards SO_2 in ambient air. It appears that Mauldin et al. [2012] have not considered

543 this correction which reduces the proposed oxidation efficiency for SO_2 of stabilized
544 Criegee intermediates from α-pinene or limonene in forested environments as well.
545 Also, our observations do not fit with diel cycles expected to arise from oxidation of
546 SO_2 by ClO, BrO, IO or OIO halogen radicals. On the other hand, CH_2OO formed
547 via photolysis of CH_2I_2 appears to be a likely candidate to explain the observed
548 increase in the OH background signal during daytime aerosol nucleation events at low
549 tide. Finally, a preliminary analysis of our measurements made during the summer of
550 2011 suggests that marine DMS emissions from biologically active waters in polar
551 latitudes may dominate H_2SO_4 formation in marine air at Mace Head during summer
552 and that SO_2 may not be the major precursor in this process. Further results will be
553 reported in a future paper.
554

Acknowledgments

Financial support for this work was provided by Science Foundation Ireland (grant 09/RFP/GEO2176), EPA Ireland (grant 2007-INF-12-S5), Higher Education Authority Programme for Research in Third Level Institutes – Cycle 4, European Commission Framework programme projects EUCAARI, (036833-2), ACTRIS (262254), and EUSAAR. This work is dedicated to Kurt and Jessica by HB.

568 **References**

569

570 Alicke, B., K. Hebestreit, J. Stutz, and U. Platt, Iodine oxide in the marine boundary
571 layer, *Nature, 397,* 572-573 (1999).

572

573 Ammann, M., R. A. Cox, J. N. Crowley, M. E. Jenkin, A. Mellouki, M. J. Rossi, J.
574 Troe, and T. J. Wallington, Evaluated kinetic and photochemical data for atmospheric
575 chemistry: Volume VI – heterogeneous reactions with liquid substrates, *Atmos. Chem.*
576 *Phys., 13*, 8045–8228 (2013).

577

578 Atkinson, R., D. L. Baulch, R. A. Cox, J. N. Crowley, R. F. Hampson, R. G. Hynes,
579 M. E. Jenkin, M. J. Rossi, and J. Troe, Evaluated kinetic and photochemical data for
580 atmospheric chemistry: Volume I – gas phase reactions of Ox, HOx, NOx and SOx
581 species, *Atmos. Chem. Phys., 4*, 1461–1738 (2004).

582

583 Berndt, T., T. Jokinen, R. L. Mauldin, III, T. Petäjä, H. Herrmann, H. Junninen, P.
584 Paasonen, D. R. Worsnop, and M. Sipilä, Gas-phase ozonolysis of selected olefins:
585 the yield of stabilized Criegee intermediates and the reactivity toward SO_2, *J. Phys.*
586 *Chem. Lett., 3*, 2892−2896 and supplement (2012).

587

588 Berresheim, H., J. McGrath, M. Adam, R.L. Mauldin III, B. Bohn, and F. Rohrer,
589 Seasonal Measurements of OH, NOx, and J(O^1D) at Mace Head, Ireland, *Geophys.*
590 *Res. Lett., 40,* 1659-1663 (2013).

591

592 Berresheim, H., T. Elste, H. G. Tremmel, A. G. Allen, H.-C. Hansson, K. Rosman, M.
593 DalMaso, J. M. Mäkelä, M. Kulmala, and C. D. O'Dowd, Gas-aerosol relationships of
594 H_2SO_4, MSA, and OH: Observations in the coastal marine boundary layer at Mace
595 Head, Ireland, *J. Geophys. Res.*, *107*(D19), 8100, doi: 10.1029/2000JD000229 (2002).
596
597 Berresheim, H., T. Elste, C. Plass-Dülmer, F.L. Eisele, and D.J. Tanner, Chemical
598 ionization mass spectrometer for long-term measurements of atmospheric OH and
599 H_2SO_4, *Int. J. Mass Spectrom.*, *202*, 91-109 (2000).
600
601 Berresheim, H., P. H. Wine, and D. D. Davis, Sulfur in the atmosphere, in
602 *Composition,Chemistry, and Climate of the Atmosphere*, edited by H. B. Singh, pp.
603 251-307, Van Nostrand Reinhold, New York (1995).
604
605 Berresheim, H., F. L. Eisele, and D. J. Tanner, Field studies of atmospheric DMS
606 chemistry using selected ion chemical ionization mass spectrometry, in
607 *Dimethylsulfide: Oceans, Atmosphere and Climate*, edited by G. Restelli, and G.
608 Angeletti, pp. 239-242, Kluwer Academic Publishers, Dordrecht (1993a).
609
610 Berndt, T., T. Jokinen, M. Sipilä, R.L. Mauldin III, H. Herrmann, F. Stratmann, H.
611 Junninen, and M. Kulmala, H_2SO_4 formation from the gas-phase reaction of stabilized
612 Criegee Intermediates with SO_2 : Influence of water vapour content and temperature,
613 Atmos. Environ., 89, 603-612 (2014).
614

615 Berresheim, H., F. L. Eisele, D. J. Tanner, D. S. Covert, L. McInnes, and D. C.
616 RamseyBell, Atmospheric sulfur chemistry and cloud condensation nuclei (CCN)
617 concentrations over the northeastern Pacific coast, *J. Geophys. Res.*, *98*, 12701-12711
618 (1993b).
619
620 Berresheim, H., and W. Jaeschke, Study of metal aerosol systems as a sink for
621 atmospheric SO_2, *J. Atmos. Chem.*, *4*, 311-334 (1986).
622
623 Bialek, J., M. Dall'Osto, C. Monahan, D. Beddows, and C. O'Dowd, On the
624 contribution of organics to the North East Atlantic aerosol number concentration,
625 *Environ. Res. Lett., 7*, doi:10.1088/1748-9326/7/4/044013 (2012).
626
627 Bohn, B., G. K. Corlett, M. Gillmann, S. Sanghavi, G. Stange, E. Tensing, M.
628 Vrekoussis, W. J. Bloss, L. J. Clapp, M. Kortner, H.-P. Dorn, P. S. Monks, U. Platt,
629 C. Plass-Dülmer, N. Mihalopoulos, D. E. Heard, K. C. Clemitshaw, F. X. Meixner, A.
630 S. H. Prevot, and R. Schmitt , Photolysis frequency measurement techniques: Results
631 of a comparison within the ACCENT project, *Atmos. Chem. Phys., 8*, 5373–5391
632 (2008).
633
634 Boy, M., D. Mogensen, S. Smolander, L. Zhou, T. Nieminen, P. Paasonen, C. Plass-
635 Dülmer, M. Sipilä, T. Petäjä, L. Mauldin, H. Berresheim, and M. Kulmala, Oxidation
636 of SO_2 by stabilized Criegee intermediate (sCI) radicals as a crucial source for
637 atmospheric sulfuric acid concentrations, *Atmos. Chem. Phys., 13*, 3865-3879 (2013).
638

639 Boy, M., M. Kulmala, T. Ruuskanen, M. Pihlatie, A. Reissell, P. P. Aalto, P. Keronen,
640 M. Dal Maso, H. Hellen, H. Hakola, R. Janssen, M. Hanke, and F. Arnold, Sulphuric
641 acid closure and contribution to nucleation mode particle growth, *Atmos. Chem.*
642 *Phys., 5,* 863–878 (2005).
643
644 Broadgate, W.J., G. Malin, F.C. Küpper, A. Thompson, and P.S. Liss, Isoprene and
645 other non-methane hydrocarbons from seaweeds: a source of reactive hydrocarbons to
646 the atmosphere, *Marine Chem., 88*, 61– 73 (2004).
647
648 Eisele, F. L., and D. J. Tanner, Ion-assisted tropospheric OH measurements, *J.*
649 *Geophys. Res., 96(D5),* 9295–9308, (1991).
650
651 Calvert, J. G., R. Atkinson, J.A. Kerr, S. Madronich, G.K. Moortgat, T.J. Wallington,
652 and G. Yarwood, *The mechanisms of atmospheric oxidation of alkenes*, Oxford
653 University Press, New York, ISBN 0-19-513177-0 (2000).
654
655 Cox, R.A., and S.A. Penkett, Oxidation of atmospheric SO_2 by products of the ozone–
656 olefin reaction, *Nature, 230,* 321-322 (1971).
657
658 Criegee, R., Mechanism of ozonolysis, Angew. Chem.-Int. Edit. Engl.,14, 745-752
659 (1975).
660
661 Fuchs, N., and A. Sutugin, Highly dispersed aerosol, in *Topics in Current Aerosol*
662 *Research*, edited by G. Hidy and J. Brock, Pergamon, New York (1971).
663

664 Davis, D. G. Chen, P. Kasibhatla, A . Jefferson, D . Tanner, F. Eisele, D. Lenschow,
665 W . Neff, and H . Berresheim, DMS oxidation in the Antarctic marine boundary
666 layer: Comparison of model simulations and field observations of DMS, DMSO,
667 $DMSO_2$, H_2SO_4(g), MSA(g), and MSA(p), *J. Geophys. Res., 103,* 1657-1678 (1998).
668
669 De Bruyn, W. J., J. A. Shorter, P. Davidovits, D. R. Worsnop, M. S. Zahniser, and C.
670 E. Kolb, Uptake of gas phase sulfur species methanesulfonic acid, dimethylsulfoxide,
671 and dimethyl sulfone by aqueous surfaces, *J. Geophys. Res., 99(D8),* 16927–16932,
672 doi:10.1029/94JD00684 (1994).
673
674 DeMore, W.B., S.P. Sander, D.M. Golden, R.F. Hampson, M.J. Kurylo, C.J. Howard,
675 A.R. Ravishankara, C.E. Kolb, and M.J. Molina, Chemical kinetics and
676 photochemical data for use in stratospheric modeling. Evaluation number *12*, JPL
677 Publication *97-4*, 1 – 266 (1997).
678
679 Eisele, F. and D. Tanner, Measurement of the gas phase concentration of H_2SO_4 and
680 methane sulfonic acid and estimates of H_2SO_4 production and loss in the atmosphere,
681 *J. Geophys. Res,. 98,* 9001–9010 (1993).
682
683 Foresman, J.B., and A. Frisch, *Exploring chemistry with electronic structure methods*.
684 Gaussian, Inc., Pittsburgh (1996).
685
686 Frisch, M.J., G. W. Trucks, H. B. Schlegel, G. E. Scuseria, M. A. Robb, J. R.
687 Cheeseman, G. Scalmani, V. Barone, B. Mennucci, G. A. Petersson, H. Nakatsuji, M.
688 Caricato, X. Li, H. P. Hratchian, A. F. Izmaylov, J. Bloino, G. Zheng, J. L.

689 Sonnenberg, M. Hada, M. Ehara, K. Toyota, R. Fukuda, J. Hasegawa, M. Ishida, T.
690 Nakajima, Y. Honda, O. Kitao, H. Nakai, T. Vreven, J. A. Montgomery, Jr., J. E.
691 Peralta, F. Ogliaro, M. Bearpark, J. J. Heyd, E. Brothers, K. N. Kudin, V. N.
692 Staroverov, R. Kobayashi, J. Normand, K. Raghavachari, A. Rendell, J. C. Burant, S.
693 S. Iyengar, J. Tomasi, M. Cossi, N. Rega, J. M. Millam, M. Klene, J. E. Knox, J. B.
694 Cross, V. Bakken, C. Adamo, J. Jaramillo, R. Gomperts, R. E. Stratmann, O. Yazyev,
695 A. J. Austin, R. Cammi, C. Pomelli, J. W. Ochterski, R. L. Martin, K. Morokuma, V.
696 G. Zakrzewski, G. A. Voth, P. Salvador, J. J. Dannenberg, S. Dapprich, A. D. Daniels,
697 Ö. Farkas, J. B. Foresman, J. V. Ortiz, J. Cioslowski, and D. J. Fox, Gaussian 09,
698 Revision A.1. Gaussian, Inc. (2009).
699
700 Glukhovtsev, M. N., A. Pross, M.P. McGrath, and L. Radom, Extension of Gaussian-
701 2 (G2) theory to bromine- and iodine-containing molecules: Use of effective core
702 potentials, *J. Chem. Phys.*, *103*, 1878-1885 (1995).
703
704 Hanson, D.R., Mass accommodation of H_2SO_4 and CH_3SO_3H on water-sulfuric acid
705 solutions from 6% to 97% rH, *J. Phys. Chem. A, 109*, 6919-6927 (2005).
706
707 Harris, E., B. Sinha, D. van Pinxteren, A. Tilgner, K. W. Fomba, J. Schneider, A.
708 Roth, T. Gnauk, B. Fahlbusch, S. Mertes, T. Lee, J. Collett, S. Foley, S. Borrmann, P.
709 Hoppe, and H. Herrmann, Enhanced role of transition metal ion catalysis during in-
710 cloud oxidation of SO_2, *Science, 340*, 727-730 (2013).
711
712 Heard, D.E., and M.J. Pilling, Measurement of OH and HO_2 in the troposphere,
713 *Chem. Rev., 103,* 5163-5198 (2003).

714

715 Huey, G.L., Measurement of trace atmospheric species by chemical ionization mass
716 spectrometry: Speciation of reactive nitrogen and future directions, *Mass Spectrom.*
717 *Rev., 26*, 166-184 (2007)

718

719 Jefferson, A., D. J. Tanner, F. L. Eisele, and H. Berresheim, Sources and sinks of
720 H_2SO_4 in the remote Antarctic marine boundary layer, *J. Geophys. Res.*, *103*, 1639-
721 1645 (1998).

722

723 Jenkin, M. E., Saunders, S. M., Wagner, V., and Pilling, M. J.: Protocol for the
724 development of the Master Chemical Mechanism, MCM v3 (Part B): tropospheric
725 degradation of aromatic volatile organic compounds, *Atmos. Chem. Phys., 3*, 181–193
726 (2003)

727

728 Kolb, C.E., R. A. Cox, J. P. D. Abbatt, M. Ammann, E. J. Davis, D. J. Donaldson, B.
729 C. Garrett, C. George, P.T. Griffiths, D. R. Hanson, M. Kulmala, G. McFiggans, U.
730 Pöschl, I. Riipinen, M. J. Rossi, Y. Rudich, P. E. Wagner, P. M. Winkler, D. R.
731 Worsnop, and C. D. O' Dowd, An overview of current issues in the uptake of
732 atmospheric trace gases by aerosols and clouds, *Atmos. Chem. Phys., 10,* 10561–
733 10605 (2010).

734

735 Kreidenweis, S. M., and J. H. Seinfeld, Nucleation of sulfuric acid water and
736 methanesulfonic acid-water solution particles: Implications for the atmospheric
737 chemistry of organosulfur species, *Atmos. Environ., 22,* 283–296 (1988).

738

739 Kroll, J. H., R.S. Shailesh, J.G. Anderson, K.L. Demerjian, and N.M. Donahue,
740 Mechanism of HOx formation in the gas-phase ozone-alkene reaction. 2. Prompt
741 versus thermal dissociation of carbonyl oxides to form OH, *J. Phys. Chem. A, 105*,
742 4446−4457 (2001).
743
744 Krouse, H.R., and V.A. Grinenko (Eds.), *Stable Isotopes: Natural and Anthropogenic*
745 *Sulphur in the Environment*, Scientific Committee on Problems of the Environment
746 (SCOPE), vol. 43, J. Wiley & Sons, Chichester (1991).
747
748 Larin, I.K., N. A. Messineva, A. I. Spasskii, E. M. Trofimova, and L. E. Turkin,
749 Measurement of the rate constants for the reactions of the $IO^{\bullet}$ radical with sulfur-
750 containing compounds H_2S, $(CH_3)_2S$, and SO_2, *J. Kinetics and Catalysis, 41*, 437-443
751 (2000).
752
753 Lewis, A.C., J.B. McQuaid, N. Carslaw, and M.J. Pilling, Diurnal cycles of short-
754 lived tropospheric alkenes at a north Atlantic coastal site, *Atmos. Environ., 33*, 2417-
755 2422 (1999).
756
757 Lin, C.T., A.R. Baker, T.D. Jickells, S. Kelly, and T. Lesworth, An assessment of the
758 significance of sulphate sources over the Atlantic Ocean based on sulphur isotope
759 data, *Atmos. Environ., 62*, 615-621 (2012).
760
761 Lin, X., and W.L. Chameides, CCN formation from DMS oxidation without SO_2
762 acting as an intermediate, *Geophys. Res. Lett., 20,* 579-582 (1993).
763

764 Liu, Y., K.D. Bayes, and S.P. Sander, Measuring rate constants for reactions of the
765 simplest Criegee intermediate (CH_2OO) by monitoring the OH radical, *J. Phys. Chem.*
766 *A, 118*, 741-747 (2014).
767
768 Mauldin III, R.L., T. Berndt, M. Sipilä, P. Paasonen, T. Petäjä, S. Kim, T. Kurtén, F.
769 Stratmann, V.-M. Kerminen, and M. Kulmala, A new atmospherically relevant
770 oxidant of sulphur dioxide, *Nature, 488,* 193-196 and supplement, (2012).
771
772 Mauldin, R., III, G. Frost, G. Chen, D. Tanner, A. Prevot, D. Davis, and F. Eisele, OH
773 measurements during the First Aerosol Characterization Experiment (ACE 1):
774 Observations and model comparisons, *J. Geophys. Res., 103*, 16713–16729 (1998).
775
776 Montgomery Jr., J.A., M. J. Frisch, J. W. Ochterski, and G. A. Petersson, A complete
777 basis set model chemistry. VII. Use of the minimum population localization method,
778 *J. Chem. Phys.*, *112*, 6532-6542 (2000).
779
780 O'Dowd, C.D., J.L. Jimenez, R. Bahreini, R.C. Flagan J.H. Seinfeld, K. Hämeri, L.
781 Pirjola, M. Kulmala, S.G. Jennings, and T. Hoffmann, Marine particle formation from
782 biogenic iodine emissions, *Nature, 417*, 632-636 (2002).
783
784 Ovadnevaite, J., D. Ceburnis, S. Leinert, M. Dall'Osto, M. Canagaratna, P. O'Brien,
785 S. O'Doherty, H. Berresheim, and C. O'Dowd, Distinct seasonal changes in marine
786 aerosol composition and its properties, *J. Geophys. Res.,* submitted (2014).
787

788 Seinfeld, J.H., and S.N. Pandis, *Atmospheric Chemistry and Physics – From Air*
789 *Pollution to Climate Change*, chapters 8 and 11, J. Wiley & Sons, New York (1998).
790
791 Saiz-Lopez, A., J. A. Shillito, H. Coe, and J. M. C. Plane, Measurements and
792 modelling of I_2, IO, OIO, BrO and NO_3 in the mid-latitude marine boundary layer,
793 *Atmos. Chem. Phys., 6*, 1513–1528 (2006).
794
795 Saiz-Lopez, A., and J.M.C. Plane, Novel iodine chemistry in the marine boundary
796 layer, *Geophys. Res. Lett.*, *31*, doi: L04112 (2004).
797
798 Saiz-Lopez, A., J.M.C. Plane, and J.A. Shillito, Bromine oxide in the mid-latitude
799 marine boundary layer, *Geophys. Res. Lett.*, *31*, doi: L03111 (2004).
800
801 Sarwar, G., H. Simon, K. Fahey, R. Mathur, W.S. Goliff, and W.R. Stockwell, Impact
802 of sulfur dioxide oxidation by Stabilized Criegee Intermediate on sulfate, Atmos.
803 Environ., 85, 204-214 (2014).
804
805 Saunders, S. M., Jenkin, M. E., Derwent, R. G., and Pilling, M.J.: Protocol for the
806 development of the Master Chemical Mechanism, MCM v3 (Part A): tropospheric
807 degradation of nonaromatic volatile organic compounds, *Atmos. Chem. Phys., 3*, 161–
808 180, (2003).
809
810 Seguin, A.M., A.-L. Norman, S. Eaton, M. Wadleigh, and S. Sharma, Elevated
811 biogenic sulphur dioxide concentrations over the North Atlantic, *Atmos. Environ., 44*,
812 1139-1144 (2010).

Schweitzer, F., L. Magi, P. Mirabel, and C. George, Uptake rate measurements of methanesulfonic acid and glyoxal by aqueous droplets, *J. Phys. Chem. A, 102*, 593–600 (1998).

Stone, D., M. Blitz, L. Daubney, N.U.M. Howes, and P. Seakins, Kinetics of CH_2OO reactions with SO_2, NO_2, NO, H_2O and CH_3CHO as a function of pressure, *Phys. Chem. Chem. Phys., 16*, 1139-1149 (2014).

Stone, D., M. Blitz, L. Daubney, T. Ingham, and P. Seakins, CH_2OO Criegee biradical yields following photolysis of CH_2I_2 in O_2, *Phys. Chem. Chem. Phys., 15*, 19119-19124 (2013).

Stone, D., L.K. Whalley, and D.E. Heard, Tropospheric OH and HO_2 radicals: field measurements and model comparisons, *Chem. Soc. Rev., 41,* 6348-6404 (2012).

Taatjes, C.A., D.E. Shallcross, and C. J. Percival, Research frontiers in the chemistry of Criegee intermediates and tropospheric ozonolysis, *Phys. Chem. Chem. Phys.,* 16(5), 1704-1718 (2014).

Taatjes, C.A., Welz, O., Eskola, A.J., Savee, J.D., Scheer, A.M., Shallcross, D.E., Rotavera, B., Lee, E.P.F., Dyke, J.M., Mok, D.K.W., Osborn, D.L., and C.J. Percival, Direct measurements of conformer-dependent reactivity of the Criegee intermediate CH_3CHOO, *Science, 340*, 177-180, DOI: 10.1126/science.1234689 (2013)

838 Tanner, D. J., and F. L. Eisele, Present OH measurement limits and associated
839 uncertainties, *J. Geophys. Res., 100(D2),* 2883–2892 (1995).
840
841 Vereecken, L., H. Harder, and A. Novelli, The reaction of Criegee intermediates with
842 NO, RO_2, and SO_2, and their fate in the atmosphere, *Phys. Chem. Chem. Phys., 14*,
843 14682–14695 (2012).
844
845 Welz, O., J.D. Savee, D.L. Osborn, S.S. Vasu, C. Percival, D. E. Shallcross, C.A.
846 Taatjes, Direct kinetic measurements of Criegee intermediate (CH_2OO) formed by
847 reaction of CH_2I with O_2, *Science, 335,* 204-207 (2012).
848
849

850 **Figure Captions**

851

852 Figure 1. Principle scheme of SI/CIMS components including air inlet (modified from
853 R.L. Mauldin III, *pers. commun.*, 2012). Inset shows details of the atmospheric
854 pressure region with reagent gas flows indicated for measurement of OH background
855 signal (both $^{34}SO_2$ and C_3H_8 are added to the sample air through the two front
856 injectors; see text). Laminar flow conditions with a central flow axis velocity of 0.71
857 m s^{-1} in both the sample and ionization tubes are generated by a 12 slpm sample flow,
858 58 slpm total flow (= sample flow plus sheath flow, the latter indicated here by
859 addition of *Air/HNO_3 mixture*), and the geometries of the sample tube (diameter 1.9
860 cm) and ionization tube (diameter 4.2 cm). The time needed (in each case starting at
861 the first injector) to reach the second injector is 73 ms, to the entrance of the
862 ionization region 115 ms, and to the aperture in front of the mass spectrometer 450
863 ms, respectively.

864

865 Figure 2. Midday (1000-1400 UTC) maximum H_2SO_4 and MSA(g) concentrations in
866 marine air at Mace Head, averaged for each month (total measurement period: May
867 2010 – August 2012).

868

869 Figure 3. Correlation between H_2SO_4 and OH (top) and between MSA(g) and OH
870 concentrations (bottom) in marine air for the period May - August 2011 (5 min
871 integrated data, daytime: 0800-2000 UTC). OH concentrations were calculated for the
872 corresponding measurement times based on concurrent $J(O^1D)$ data and the $J(O^1D)$-OH
873 relationship for marine air previously established in Berresheim et al. [2013].

874

875 Figure 4. (top) SO_2 mixing ratios (1 hour signal integration) measured in marine air
876 between May – August 2011 (average: 160 (± 50) pptv; detection limit: 25 pptv,
877 indicated by red line); (bottom) Condensational sink (CS; 5 min integration)
878 calculated for H_2SO_4 (see text).
879
880 Figure 5a. Example of observed ambient H_2SO_4 concentration in comparison with
881 H_2SO_4 mass balance values calculated from eq. (1) for 18 June 2011. Air masses
882 originated from polar regions between Greenland and Iceland exhibiting strong
883 biological activity in surface waters. The OH concentrations used for the calculations
884 were derived from the OH-J(O^1D) relation established for the marine sector
885 [Berresheim et al., 2013] (continuous 5 min time resolution). (top) Mean discrepancy
886 factor of 7.0 between midday (1000-1400 UTC) observed and calculated [H_2SO_4].
887 (bottom) Signal counts obtained for OH measurement (OH plus background) and
888 background mode only (cycle: 5 min during each 30 min period).
889
890 Figure 5b. Example of relatively small discrepancy between measured and calculated
891 H_2SO_4 based on eq (1) for 10 May 2011 (ratio 1.8). Air mass origin was mainly from
892 temperate North Atlantic in connection with anticyclonic conditions. For further
893 explanations see Figure 5a caption and text.
894
895 Figure 6. Mean half-hour values measured in marine air of the OH mode raw signal at
896 m/z 99 (blue line), total background mode raw signal at m/z 99 (red line), OH mode
897 signal minus background mode signal (green line = net signal counts corresponding to
898 the ambient OH concentration), signal counts at m/z 99 due to ^{34}S mass fraction of

899 ambient H_2SO_4 (black dashed line = signal(m/z 97)*0.044), OH mode background
900 signal with ^{34}S fraction of ambient H_2SO_4 subtracted (red dashed line).
901
902 Figure 7. Transition state geometries for ClO, BrO, IO and OIO + SO_2.
903
904 Figure 8a. Example observation showing relationships between aerosol nucleation
905 events at low tide, OH concentrations, and OH background (BG) signal (due to X-
906 compound). (top) H_2SO_4 and MSA(g) concentrations (30 s integration), tidal height,
907 and total particle number concentration N_p > 3 nm diameter (30 s integration)
908 measured with a condensation particle counter (CPC; TSI 3025). (bottom) OH
909 concentrations (5 min; black dots), count rates for OH+BG and BG only (non-OH)
910 signals (30 s), and ozone photolysis frequency, $J(O^1D)$.
911
912 Figure 8b. Example of increased OH concentrations and OH background signal (BG)
913 during two aerosol nucleation events at low tide under marine sector conditions.
914 Symbols as in Figure 8a.
915

Table 1. Molecular parameters and energies for transition state theory calculations (see text for theoretical methods). The symbol # indicates a transition state.

Species	Transition state geometry[a]	Rotational constants / GHz	Vibrational frequencies / cm^{-1}	Relative energy[b] / kJ mol^{-1}
ClO		18.03	829	-
SO_2		58.67, 10.17, 8.667	508, 1146, 1334	-
$ClO\text{-}SO_2^{\#}$	Cl: 2.906, 0.862, -0.283 O: 1.988, -0.503, -0.103 S: -0.021, -0.255, -0.325 O: -0.353, 1.084, 0.116 O: -0.553, -1.414, 0.357	8.227, 1.831, 1.540	248*i*, 73, 135, 270, 296, 492, 720, 1113, 1303	24.1
BrO		12.50	713	-
$BrO\text{-}SO_2^{\#}$	Br: -0.048, 0.360, 0.367 O: 0.235, -0.502, 1.910 S: 1.906, 0.0189, 3.011 O: 2.914, 0.483, 2.075 O: 2.140, -1.167, 3.803	8.138, 1.128, 1.011	239*i*, 63, 114, 227, 280, 494, 625, 1115, 1302	20.4
IO		9.844	649	-
$IO\text{-}SO_2^{\#}$	I: 1.387, 0.0252, 0.0250 O: -0.292, -0.940, -0.130 S: -2.056, 0.068, 0.307 O: -1.803, 1.417, 0.167 O: -2.984, -0.780, 0.412	8.050, 0.875, 0.806	258*i*, 73, 109, 222, 292, 495, 613, 1107, 1288	7.3
OIO		18.31, 7.054, 5.092	273, 809, 831	-
$OIO\text{-}SO_2^{\#}$	S: -0.005, 0.236, 0.0738 O: 0.210, 0.766, 1.416 O: 1.111, -0.069, -0.803 I: -1.644, 3.069, 0.096 O: -0.961, 1.427, -0.805 O: -0.190, 4.124, 0.404	4.572, 0.871, 0.839	304*i*, 29, 79, 129, 202, 261, 417, 495, 547, 810, 1064, 1247	50.1

[a] Atomic positions in Cartesian coordinates (Å)

[b] above the reactants, including zero-point energies

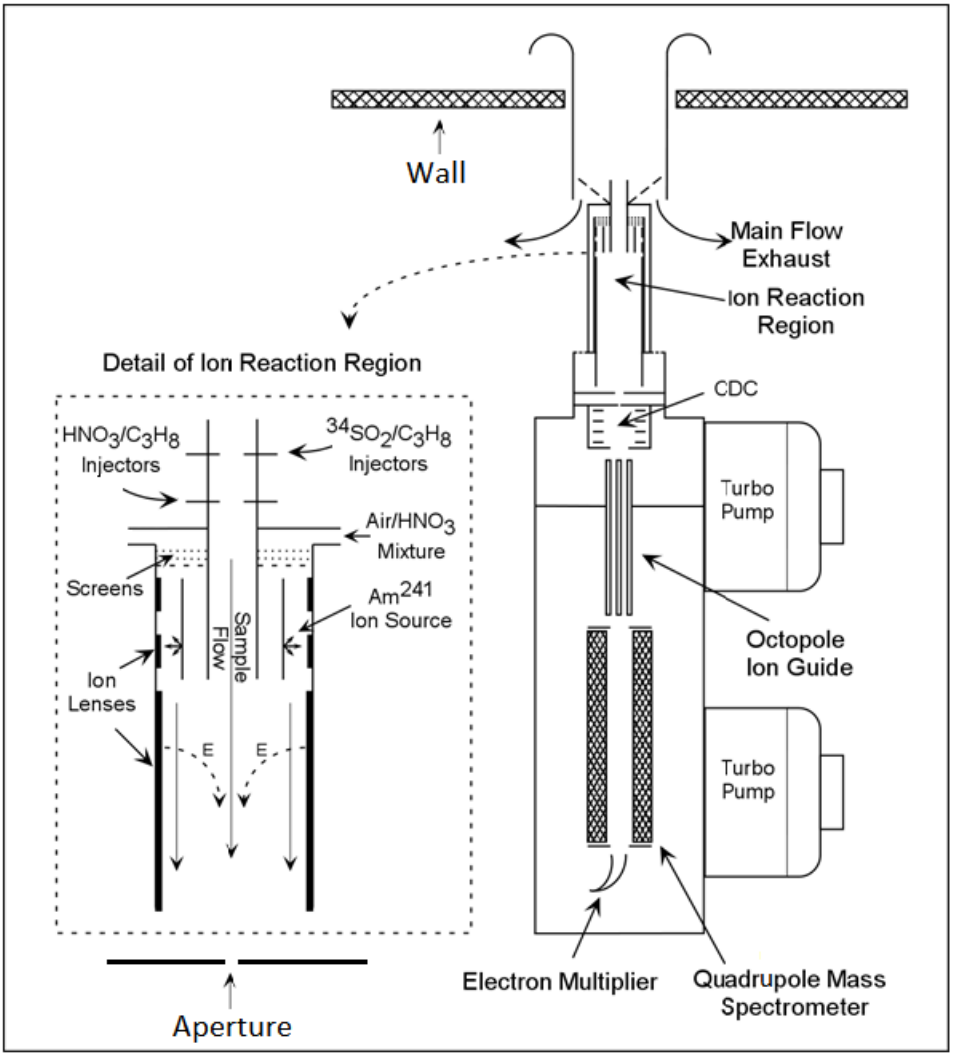

927

928

929 Figure 1

930

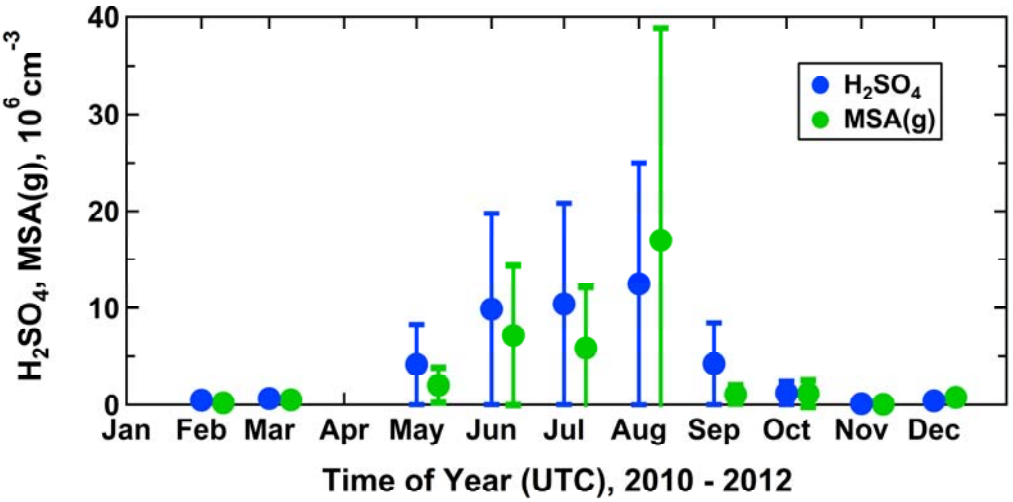

931

932

933 Figure 2.

934

935

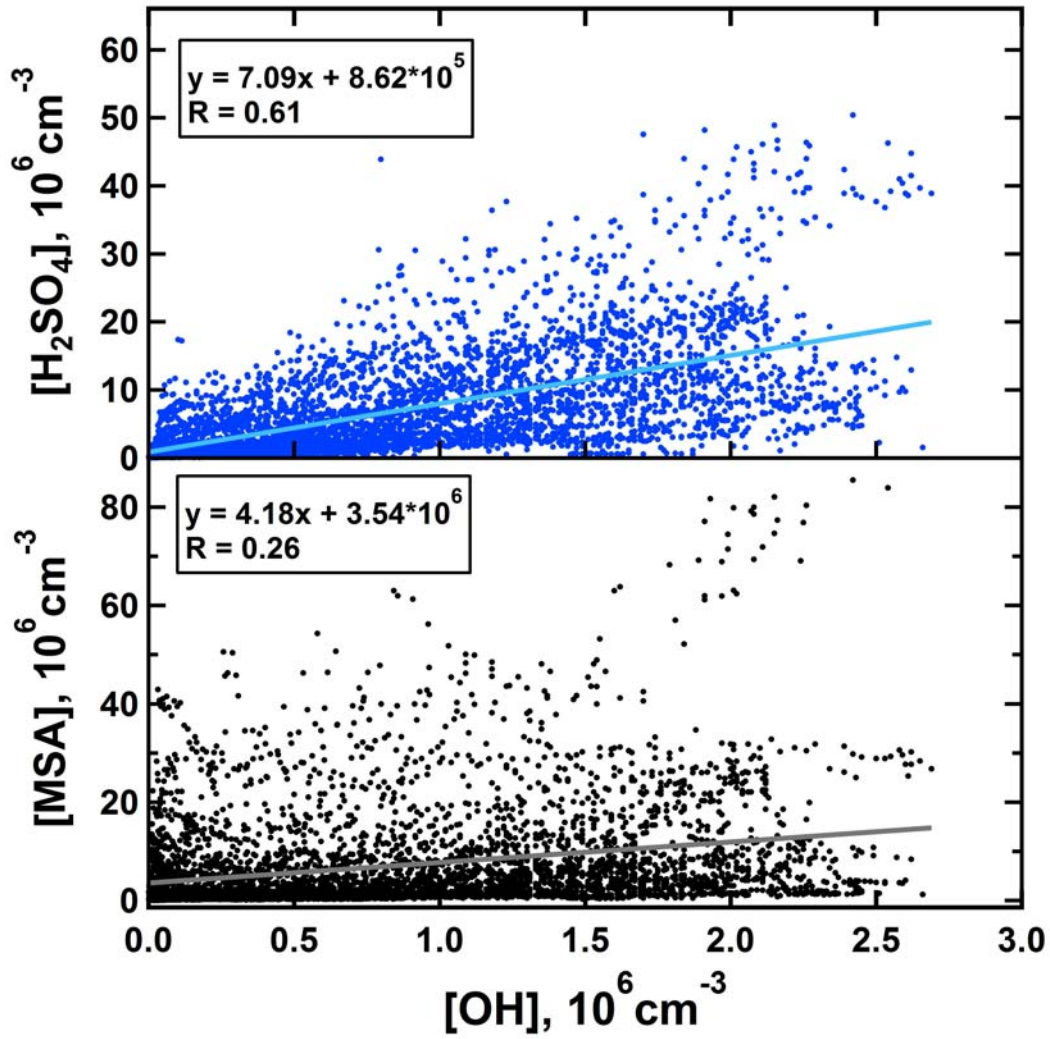

936

937

938 Figure 3.

939

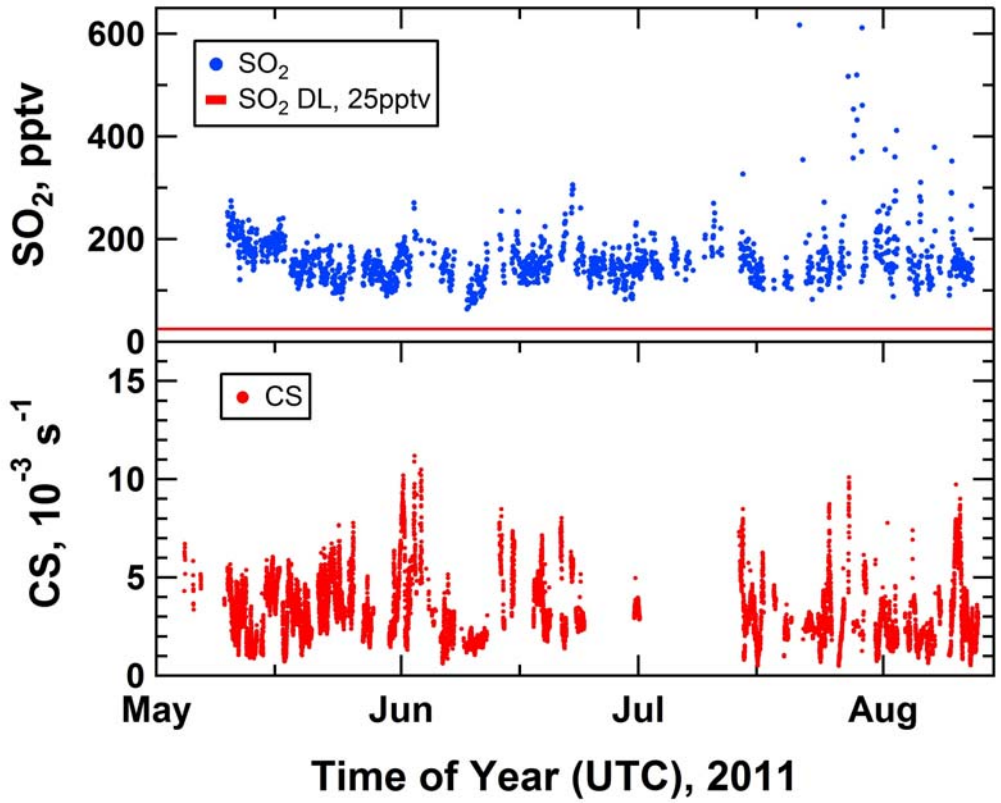

940

941 Figure 4.

942

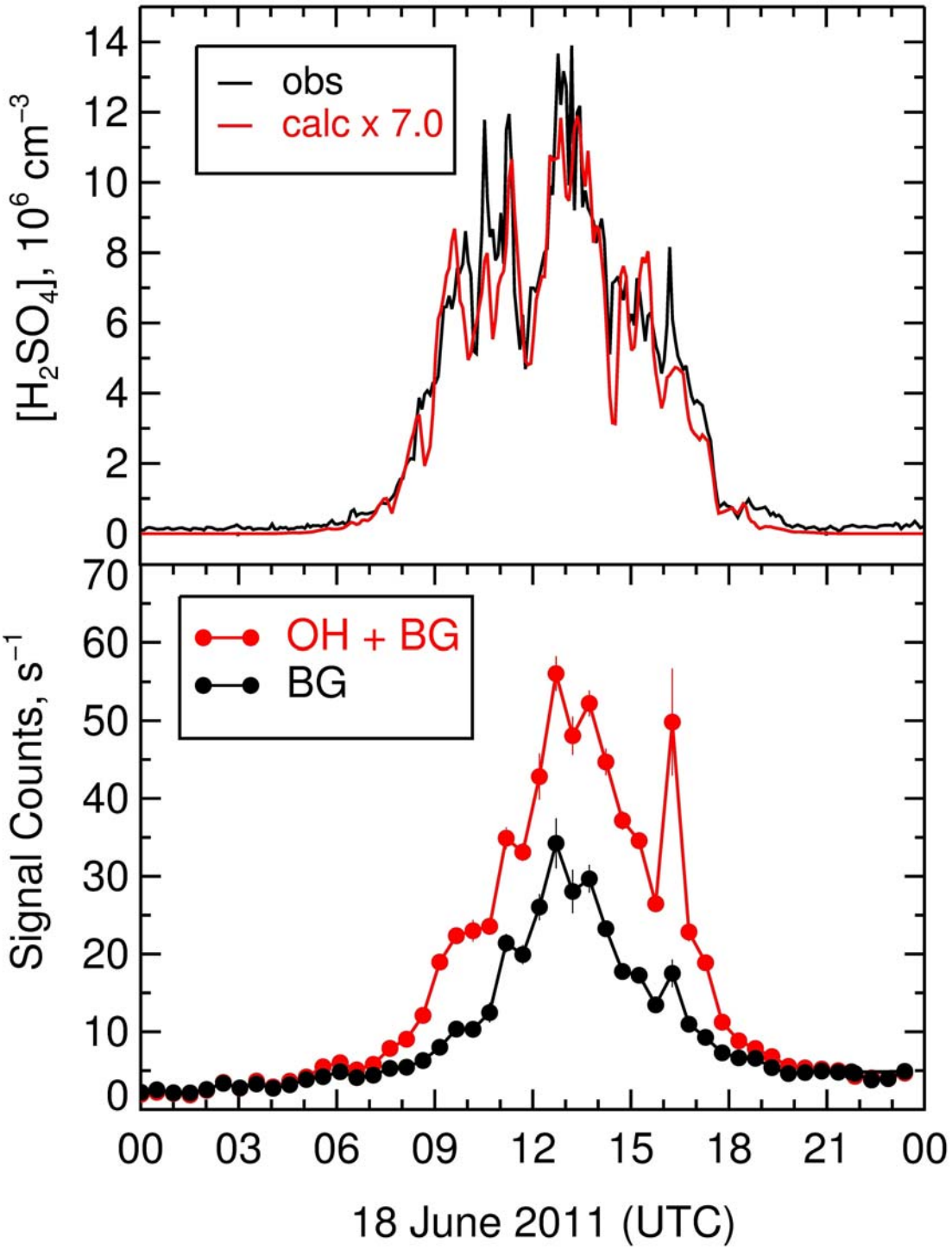

943

944

945

946 Figure 5a.

947

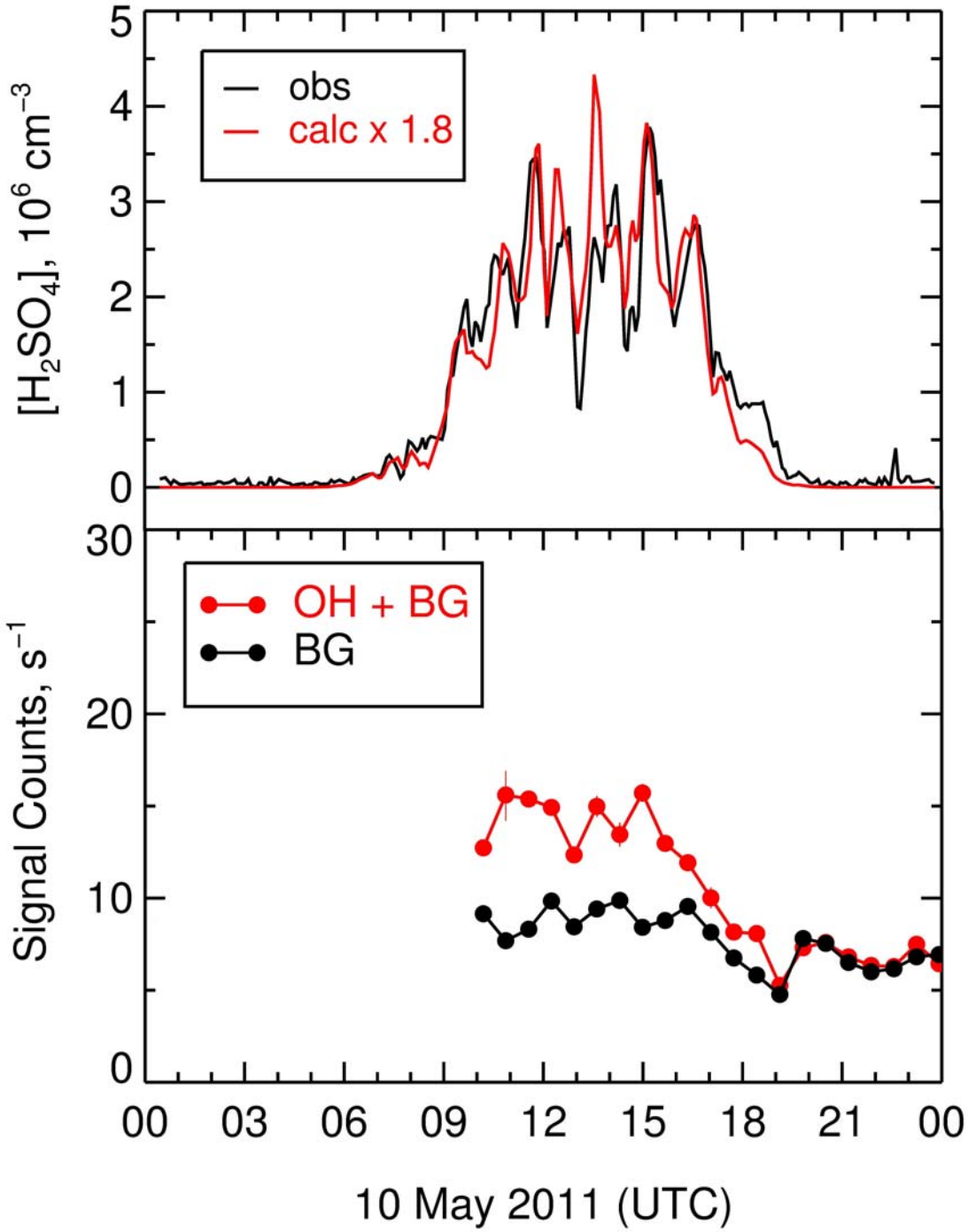

948

949 Figure 5b.

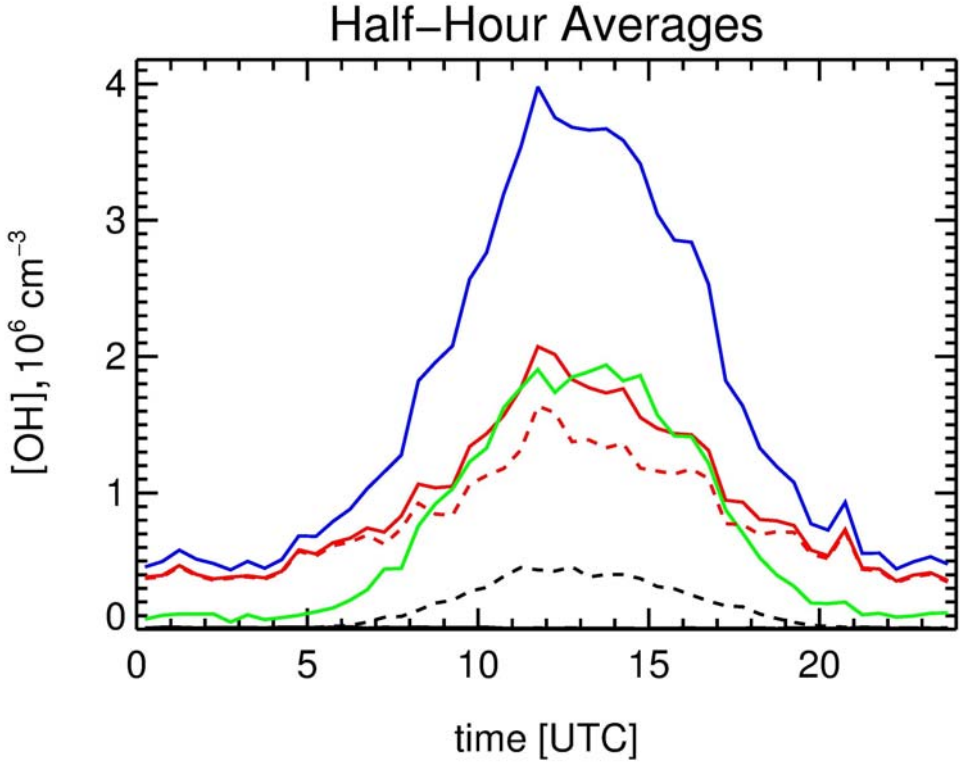

950

951 Figure 6.

952

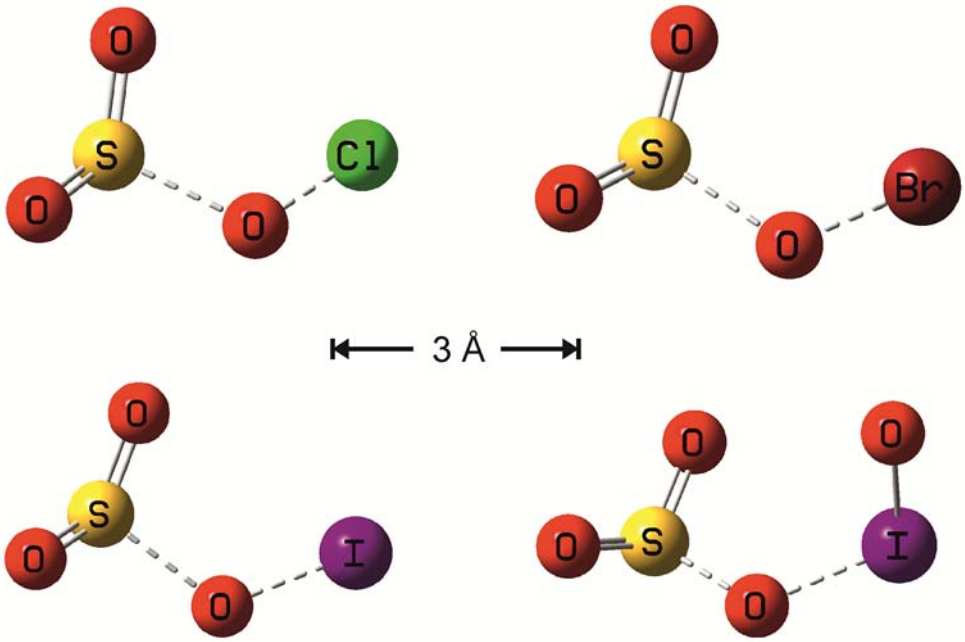

Figure 7.

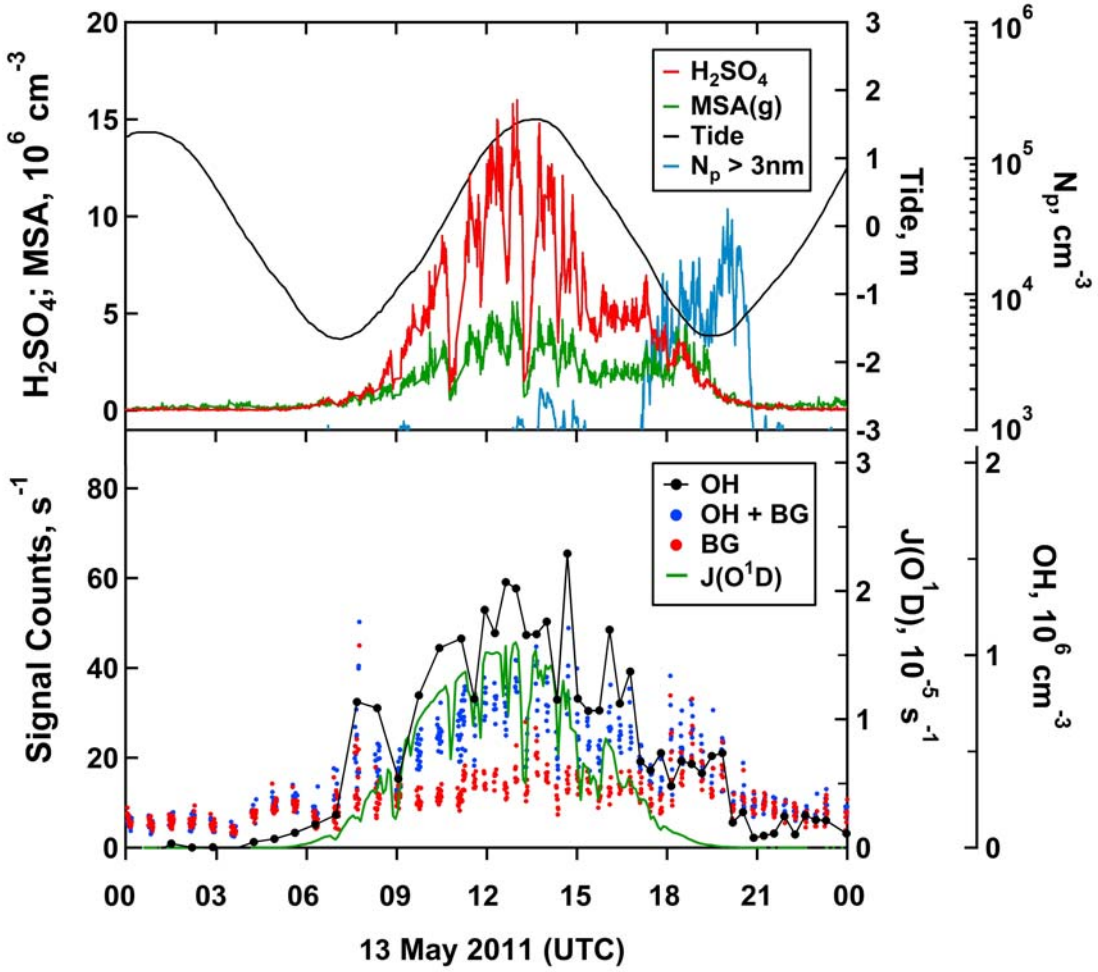

958

959 Figure 8a.

960

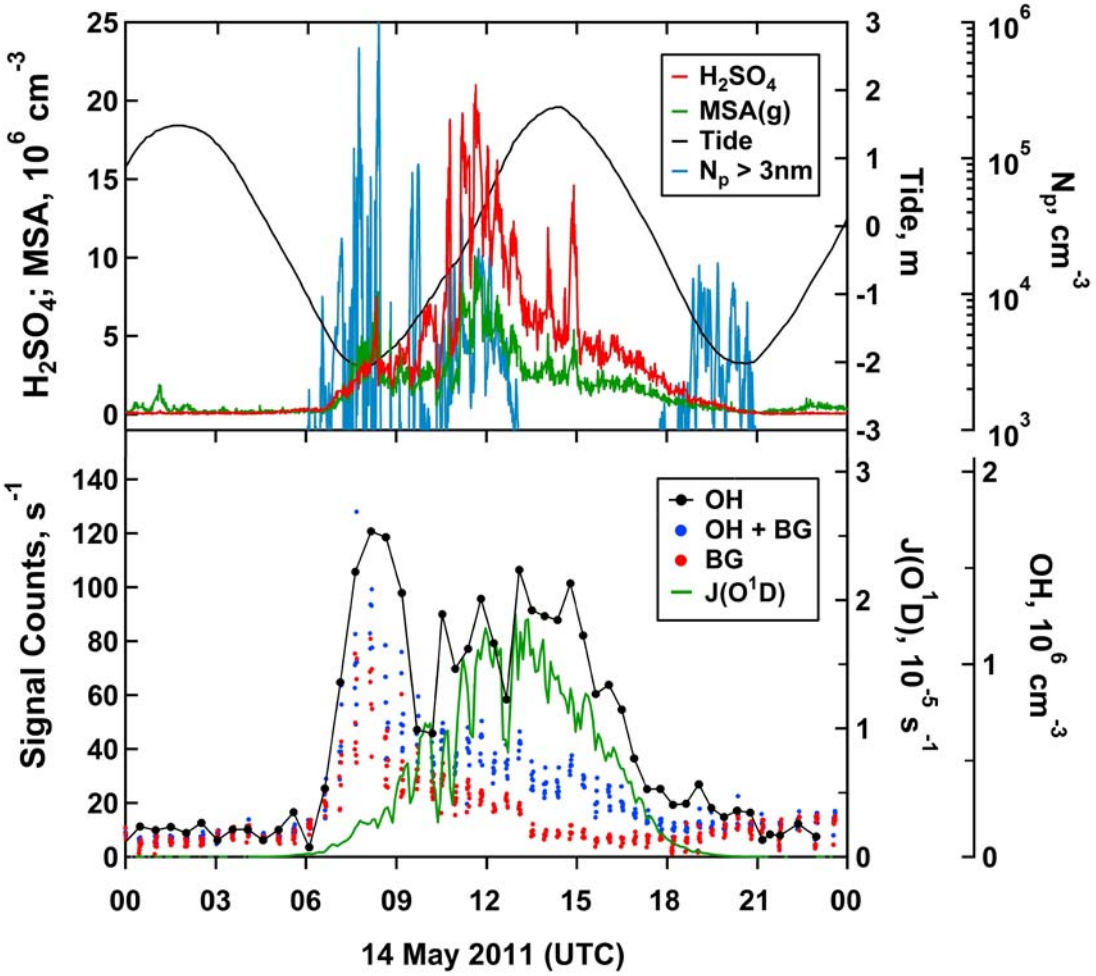

961

962 Figure 8b.